A.C. Plasma Anemometer for Hypersonic Mach Number Experiments

Eric H. Matlis* and Thomas C. Corke†

University of Notre Dame, Notre Dame, Indiana, 46556, USA

Sivaram P. Gogineni‡

Innovative Scientific Solutions, Inc., 2766 Indian Ripple Road, Dayton, Ohio, 45440, USA

A working prototype of a miniature 2 MHz a.c. driven, weakly-ionized plasma anemometer for measurements at hypersonic Mach numbers has been developed. This device uses a plasma discharge between two encapsulated electrodes as the primary sensing element. The discharge is driven by a low power (less than 5 Watt) a.c. source at voltages on the order of 350 at atmospheric pressure with electrode gaps of 0.003 in. (0.0762 mm). The discharge has demonstrated sensitivity to mean and dynamic mass-flux variations at Mach numbers up to 5.0 and at frequencies of 200 kHz. In principle, a frequency response in excess of 1 MHz is possible. The advantages of the plasma anemometer are that it requires no frequency compensation up to its a.c. carrier frequency, has an amplitude-modulated output that has excellent common-mode rejection with a signal-to-noise ratio that is much better than a hot-wire, is robust with no sensor element to break, can have a small spatial volume, and is insensitive to temperature variations making calibration easier than thermal-based sensors. The probe has also been tested for repeatability and has shown no hysteresis in its dependence to mass-flux. This sensor has applications for measurements in gas-turbine machinery, shock tubes, shock-boundary layer experiments, high-enthalpy hypersonic flows, and in plasma tunnels.

I. Introduction

In recent years there has been a renewed interest in obtaining measurements in high-speed, high-enthalpy flows where high-bandwidth sensitivity to mass-flux is desirable with a sensor that combines robustness and small measurement volumes. The objectives of these research areas include clarifying the mechanisms of stability and transition to turbulence of high-speed compressible boundary layers, the unsteady aspects of shock-boundary-layer interactions at high Mach numbers, and high-speed flows in compressors and turbines where high shear rates and velocity gradients complicate traditional measurement methods. Improved predictions of transition Reynolds number are needed in aeronautics applications such as high-speed vehicles or Earth re-entry systems. Shock interactions are critical to supersonic inlets of air breathing engines of supersonic aircraft. The rotating-machinery class of flows are important to the design of a new and efficient generation of turbofan engines.

Thermally based sensors are the de-facto standard for high-bandwidth measurements where high spatial sensitivity is required, such as the flows considered here. These sensors, which include hot-wires and hot-film sensors, rely on the convection of heat as the main sensing mechanism and are severely limited in natural frequency response due to their thermal inertia. They respond to flow fluctuations as a first-order system with corner frequencies of less than 1 kHz. As a consequence, all hot-wire based sensors are usually frequency compensated with an external circuit in a feed-back or feed-forward mode, nevertheless the bandwidth of

*Post-Doctoral Research Assistant, AME dept., AIAA student member.

†Clark Chair Professor, Director FlowPAC, Associate Fellow AIAA

‡Vice President ISSI, AIAA Fellow.

these compensated circuits is typically less than 500 kHz. Additional difficulties with hot-wire sensors are their fragility and lack of robustness. They are difficult to calibrate because of their temperature dependence, and are generally not suitable to high-enthalpy, high Mach-number flows.

II. Plasma Anemometer Background

As far back as 1934, there was the suggestion by Lindvall[1] that an electric discharge could be used in an anemometer application. He used a d.c. glow discharge to measure velocities in the wake of a cylinder. A glow discharge is one regime in a voltage-current relation of a gas exposed to a strong electric field. In 1941, a group of investigators in Germany became interested in Lindvall's work and began studying the use of electric discharge techniques to measure turbulence in air. This work is best summarized by Fucks (1947).[2]

In the U.S., Mettler (1949)[3] succeeded in developing a d.c. glow discharge anemometer that had low noise. He demonstrated its use in a Mach 1.6 flow, and indicated that this did not represent a velocity upper limit. He also developed a quantitative theory for the response of the glow discharge to an air-flow. In this, he found that the effects of temperature were not appreciable.

Werner (1955)[4] also met some success in developing a corona discharge anemometer. His design was used to measure a Mach 0.8 flow, and was reported to have an un-compensated frequency response of 100 kHz or more.

The greatest success in the early development of the glow discharge anemometer was with Vrebalovich (1954).[5] He investigated both d.c. and a.c. glow discharge designs. In particular, the a.c. design was found to be superior with regard to degrading of the electrodes over time. With an a.c. driven probe, he performed boundary layer measurements for Mach numbers from 1.3 to 4. His a.c. anemometer used a 700 kHz carrier frequency. The glow discharge "plasma" was formed in the gap between two electrodes. Typical gap distances were 0.0762 mm.

Recent work on an a.c. plasma anemometer has verified the advantages of using a.c. as opposed to the d.c. mode of operation, and demonstrated a sensitivity to variations in both mean and time-resolved mass-flux. In addition, the useful range of the sensor has been extended to Mach 5. Further details on these results can be found in Matlis et al.[6]

III. Design Objectives

To address the known limitations of thermal-based sensors in achieving both high static sensitivity, frequency response, and durability for high-enthalpy hypersonic flows, a design for a modern a.c.-plasma anemometer for hypersonic measurements was undertaken. This probe was designed to have a frequency response of at least 1 MHz, and capitalized on several significant advantages inherent to the plasma anemometer:

- a robust design with no sensor element to break,
- a small measurement volume produced using narrow (0.0254 mm) electrode gaps,
- a natively high frequency response up to its a.c. carrier frequency, requiring no frequency compensation,
- an amplitude modulated output providing excellent common-mode rejection, and large signal-to-noise ratio that is much better than a hot-wire, and
- an insensitivity to temperature variations making calibration in compressible flows easier than thermal-based sensors.

Recent work with plasma actuators (Post 2003[7]) has shown the advantages of using a.c. voltage sources over d.c. for plasma generation in air to avoid the effects of sputtering and electronic noise. It is well understood (Enloe et al. 2003[8]) that the plasma produced by the a.c. is a function of the time rate of the change of the voltage, and that its stability improves at higher dE/dt.

The objective for the plasma anemometer is to use a high carrier frequency to maximize its frequency response, to the order of 1 MHz. The frequency response should be related to the ion mobility. According to the mobility data given by Loeb,[9] the velocity of positive ions in pure dry air is given by the relation:

$$v = \chi * k. \tag{1}$$

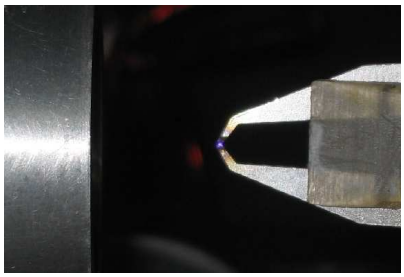

Figure 1. Plasma probe at exit of a Mach 2 nozzle.

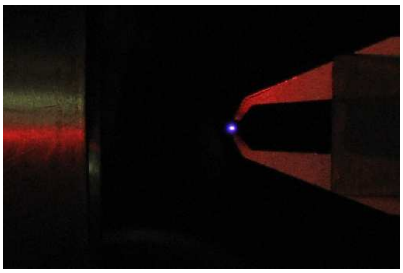

Figure 2. Plasma probe in darkened lab.

where:

v = is the positive ion velocity in cm per second,

χ = the field strength in volts per cm, and

κ = a proportionality constant for the ion mobility in $\frac{cm/s}{volt/cm}$.

From ion mobility data,[9] with $\kappa = 1.6\ \frac{cm/s}{volt/cm}$ for air, one can estimate that an average ion velocity of 1000 m/s could be attained in a gap of 0.08 mm (.003 in.) at atmospheric pressure for a gap voltage of 500 V_{rms}. This gives the time for an ion to cross the gap of approximately 10^{-8} seconds. This happens at each half cycle of the a.c. input to the anemometer, and sets an upper limit on the frequency response of approximately 15 MHz! Practically speaking, the upper frequency response limit will be set by the electronics, not by the ion mobility.

IV. A.C. Plasma Sensor Geometry

The plasma device consists of two metal electrodes captured by a plastic holding device designed to maintain a fixed gap. The electrodes are aligned so that a small gap is formed at the tips, on the order of 0.0254 mm. Pictures of the device operating downstream of a Mach 2 nozzle can be seen in Figures 1 and 2. The thickness of the electrode where the plasma forms is made thin (0.23 mm) to minimize blockage, and allow for good spatial resolution.

A high-power, high frequency amplifier drives a step-up transformer to produce the high a.c. voltages necessary to strike the plasma. The frequency of the carrier used to drive the plasma is typically over 2 MHz. Although starting voltages are high (on the order of 1 kV rms), power levels are quite low, as low as 1 Watt. Once the plasma has started, the voltage necessary to sustain it reduces to roughly one third of the starting value and the power must be quickly reduced to avoid burning out the electrodes. This is necessary because of the small size of the sensor portion of the probe which has small thermal mass.

V. Mechanism for Flow Sensitivity

The effect the flow has on the plasma device is measured as a time-varying voltage modulation that changes with flow speed. Once the gas in the gap breaks down and conducts, the current flow across the gap results in a voltage drop which can be measured at the powered electrode and which can be correlated to a flow velocity (or mass-flux). This measurement is made through a "T"-junction at the cable leading to the powered electrode. A high-voltage 1000:1 high-bandwidth attenuation probe can be used to send this voltage to an oscilloscope or digitizer. The change in plasma voltage as the flow in the gap varies can be explained by examining the flow's effect on the current-carrying particles in the electrode gap. The ionized and meta-stable species involved in the glow-discharge experience a drag force in the direction of the flow. This drag will collectively deflect the trajectory of the plasma particles towards the downstream edge of the electrodes as they traverse the gap. Inevitably, some of these particles are swept out of the gap entirely, at which point they no longer contribute to the current flow in the device. This is registered as a rise in voltage. A theoretical basis for this process was attempted by Mettler[3] in his analysis of a d.c. glow discharge and his depiction of this process is reproduced in Figure 3.

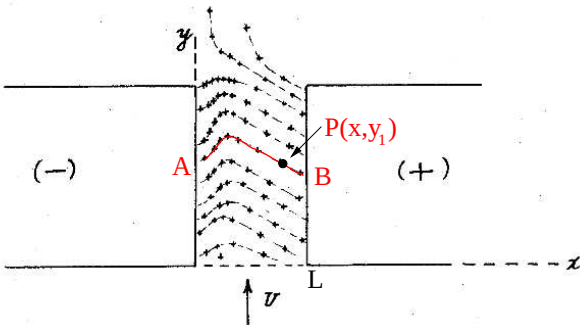

Figure 3. Drift Trajectory of Ions in Gap (Mettler[3]).

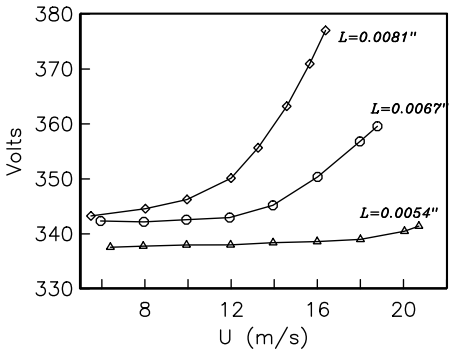

Figure 4. Plasma sensor calibration for different electrode gap distances (Mettler[3]) .

The ion trajectory is deflected in the direction of the flow due to aerodynamic drag. A number of ions nearest the downstream edge of the electrodes are shown being swept out of the gap. Direct observation supports the mechanism proposed in this figure and has confirmed the presence of an optically active wake of charged particles that continues to glow several inches downstream of the gap in a Mach 1.4 flow.

A reasonable simplification of the glow discharge process as proposed by Mettler is to assume that the electron drift is only in the x-direction as shown in Figure 3. This can be justified comparing the relative drift velocities of the electron and positive ions in an electric field. By considering a 4 mm. electrode spacing at a potential of 6kV, the ion drift velocity will be approximately 240 m/s.[9] In contrast, experimental measurements (Loeb[9]) indicate the electron drift velocity will be approximately 83,000 m/s, or 350 times larger! Thus only the ions are affected by the flow velocity, U.

Based on this assumption that electron mobility is not a factor, Mettler derived an expression relating the current flow to the ionization of the plasma and the gap dimension L. This analysis started from a "continuity" relation for electrons that considered the ion generation along a path $\bar{AB}$. At any point P along this path, the number of ions produced per unit volume via electron collision depends on the ionization coefficient $\alpha(x, y_1)$ at that location. This analysis is summarized below in Equation 2:

$$n_e(y) = \gamma(y) \int_0^L \alpha(x, y_1) n_e(y_1) e^{\int_0^x \alpha(x,y_1)dx} dx. \tag{2}$$

where

n_e = total no. of electrons per cm^2 of cathode per sec.

$\alpha(x, y_1)$ = the ionization coefficient at P, and

γ = proportionality constant that depends on the energy of the positive ions and relates the number of electrons released from the cathode to the number of ions striking it.

In order to solve Eq[2], a knowledge of the path $\bar{AB}$, and the relation between $\alpha(x, y_1)$ and $n_e(y)$ are required, which is not possible in a closed form. However we can note that $n_e(y)$ is a function of the electrode gap (L), and ionization factor, $\alpha = f(E, P_s)$, where E is the electric field strength, and P_s the air pressure.

Knowledge of $n_e(y)$ would allow calculation of the currents in the anode and cathode leads as a function of velocity at constant voltage. Such expressions could then be solved to give voltage as a function of velocity at constant current. Given the assumptions made, such calibration relations suggest a form that can be used to optimize the sensor, as well as provide a calibration equation with free coefficients (similar to King's Law with hot-wires) that can be determined in least-square-fit analysis of experimentally derived velocity-voltage data pairs.

An example of the calibration results from Mettler[3] are shown in Figure 4. This shows output d.c. voltage versus mean velocity for different gap spacings between the electrodes. This illustrates an increased sensitivity at lower velocities with larger gap distances. This is consistent with Eq[2] in which the integration is on x appears in both linear and exponential terms. The trends in the calibration curves are a composite of

these two functionals, with the exponential dependence being more dominant term at the larger gap spacings. This dependence can be exploited to provide different static sensitivity for different ranges of velocities.

A. Static Response

The static response of the sensor is characterized by the amplitude of the carrier driving the plasma. This magnitude is a function of the current lost due to aerodynamic drag. This drag results in a net loss of current as plasma is swept out of the gap which causes an increase in the necessary current density to sustain the plasma, which in turn causes an increase in the voltage measured across the plasma. A rough analogy can be made with a variable resistor; as the flow speed increases and additional current is lost, the internal resistance of the plasma increases. At the limit, at some sufficiently high external air flow rate, enough plasma is convected out of the gap to extinguish the glow discharge, which causes the voltage at the powered electrode to rise sharply. The voltage at the powered electrode is a maximum when no glow discharge exists in the gap because no current is flowing to produce a voltage drop.

B. Dynamic Response - Amplitude Modulated Carrier

The dynamic response of the sensor is characterized by an amplitude-modulation of the carrier. As the air flow through the gap fluctuates, the amount of ions swept out of the gap also fluctuates. Fluctuation energy in the flow is therefore a modulating influence on the carrier. These fluctuations are present as spectral energy bands to the side of the carrier, i.e. in the side-bands. The separation from the carrier of the side band is equal to the modulating frequency. Either side-band carries the same information. This side-band behavior is typical of an amplitude-modulated waveform and can be demodulated to produce a voltage time-series of the modulating disturbance. This is illustrated in Figure 5.

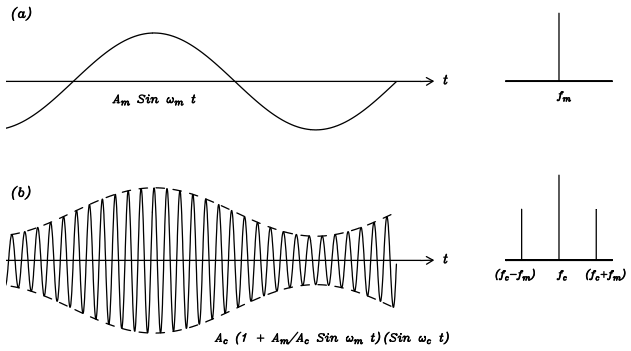

Figure 5. Illustration of the effect of a sinusoidal flow disturbance, $U(t)$, (a) that leads to an amplitude modulation of the plasma sensor carrier a.c. signal (b).

In the illustration, the a.c. carrier is denoted as f_c. Time-dependent velocity fluctuations, modeled as a sinusoidal disturbance of frequency f_m, affect the carrier amplitude across the electrodes by modulating it at the frequency of the disturbance. The mathematical expression of this response is described by a linear modulator. The general expression for the output of a linear amplitude modulator with a sinusoidal modulation input is:

$$E = E_o(1 + m\sin\omega_m t)\sin(\omega_c t + \phi). \tag{3}$$

where E_o is the peak amplitude of carrier signal, ω_m is the modulating signal frequency (rad/s), ω_c is the carrier frequency (rad/s), m is the modulation index, ϕ is an arbitrary carrier phase angle (rad), and t is time (s).

Expansion of Eq[3] gives

$$E = E_o\sin(\omega_c t + \phi) + \frac{mE_o}{2}\cos\left[(\omega_c - \omega_m)t + \phi\right] - \frac{mE_o}{2}\cos\left[(\omega_c + \omega_m)t + \phi\right]. \tag{4}$$

We note that the carrier signal is reproduced exactly as if it carried no modulation. The carrier in itself does not contain any information with regard to the time-varying component of flow, only of the time-mean

state of the plasma sensor. The second and third terms in Eq[4] represent sideband signals produced in the modulation process. These signals are displaced from the carrier signal in the frequency spectrum. They appear as spectral peaks on each side of the carrier peak, at frequencies corresponding to $f_c + f_m$ and $f_c - f_m$. This is illustrated in the lower right side of Figure 5. The magnitudes of the sideband peaks are equal and proportional to the modulation index m, where m is defined as

$$m = \begin{cases} \dfrac{E_{max} - E_o}{E_o}; & \text{positive modulation} \\ \dfrac{E_o - E_{max}}{E_o}; & \text{negative modulation} \end{cases}, \tag{5}$$

In Eq[5], E_{max} is the peak amplitude of modulated carrier and E_o is the peak amplitude of the unmodulated carrier. The modulation index in this case represents the energy carried by the fluctuation disturbance relative to the plasma carrier amplitude. This is directly related to the velocity fluctuations.

VI. Results

Experiments were conducted with the plasma sensor to document it static sensitivity and frequency response. The configuration for these measurements is shown in Figure 6. The probe was mounted on a mechanical vernier slide in order to traverse the probe in the wall-normal direction. This was used to make measurements in the turbulent boundary layer on the floor of a Mach 1.4 test section. A clear acrylic section measuring 4 in. x 5 in. (10.16 cm x 12.7 cm), was inserted into the tunnel floor to ensure the probe did not short during near-wall measurements. The photograph on the right part of Figure 6 shows the plasma when viewed through the clear wall panel in the darkened lab.

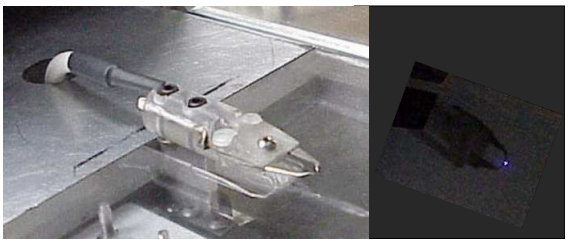

Figure 6. Plasma velocity sensor used in Mach 1.4 boundary layer measurement (left). Probe running in darkened lab (right).

A. Cylinder Wake Measurements

The vortex shedding in wakes of cylinders was used as a measurement frequency standard for the plasma sensor frequency response analysis. This capitalizes on the reproducible nature of coherent disturbances that could also be verified by independent hot-wire measurements. A series of tests were conducted at increasingly higher speeds to document the frequency response of the sensor. Sample results of this are presented in Figure 7. All measurements by the plasma probe were verified with a hot-wire anemometer for consistency.

The plots in Figure 7 correspond to varying the free-stream speed over the cylinder. The results for the minimum speed are shown in the bottom part of the figure. This corresponds to 120 m/s. At this speed, the cylinder vortex shedding occurs at 17 kHz. The spectra of the output from the plasma sensor indicates side-band peaks at 17 kHz shedding frequency and its harmonic at 34 kHz. The harmonic, which was also seen in a separate hot-wire study, is due to the asymmetric shedding process on the cylinder.

The top plot corresponds to 160 m/s. The cylinder shedding frequency at this speed is 27 kHz. The spectra of the output from the plasma sensor in this case indicates side-band peaks at 27 kHz and its harmonic at 54 kHz. The gradual shift in frequency with each flow speed from the lowest to the highest value results from the near-constant Strouhal number dependency of the shedding process, and demonstrates the response of the plasma sensor to this variation.

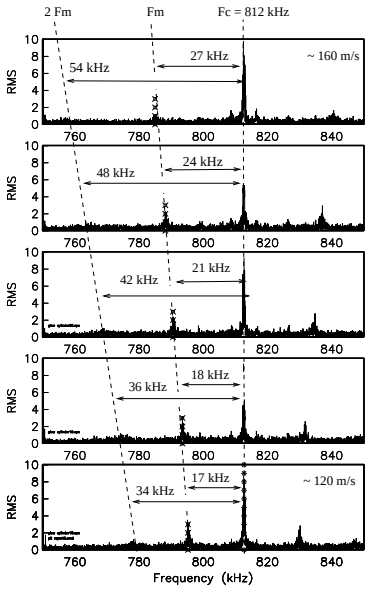

Figure 7. Spectra of plasma sensor output corresponding to measurement of velocity fluctuations due to cylinder wake shedding in a range of speeds from 120-160 m/s.

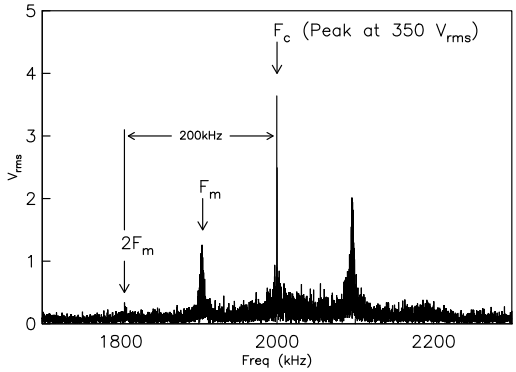

Figure 8. Spectra of plasma sensor output corresponding to measurement of velocity fluctuations due to cylinder wake shedding at Mach 0.9.

The highest frequency measured to date was at 200 kHz. This occurred at the harmonic of the wake shedding behind a 0.02 in. (0.508 mm) cylinder at a transonic Mach number of approximately 0.9. The spectra of the output from the plasma sensor is shown in Figure 8. The power used by the anemometer for these results was roughly 5 Watts. Similar measurements were successfully made at speeds as high as Mach 5.

B. Turbulent Boundary Layer Measurements

The plasma probe was used to make measurements in the turbulent boundary layer on the floor of a Mach 1.4 test section. The setup for this was shown in Figure 6. The results of this are shown in Figures 9 and 10. Figure 9 shows the variation with distance above the wall of the r.m.s. amplitude of the a.c. carrier (f_c), which is proportional to the mean mass-flux. This has the characteristic shape we expect in a boundary layer, with a minimum at the wall, and an asymptote to a constant value in the free-stream. With a documented boundary layer, this profile would represent a calibration of the sensor to mean mass-flux.

Figure 10 shows the wall-normal variation of the r.m.s. amplitude of the energy in frequencies that are at the side bands of the carrier. In contrast to the cylinder wake experiments, the energy in the side-band frequencies are broadly distributed for the turbulent flow. The curve through the data is intended to guide the eye. In general, it shows a reasonable trend, which is a minimum fluctuation level at the wall, a maximum away from the wall, and a then an asymptote towards the free-stream fluctuation level.

VII. Real Time Processing

A key requirement to make this device a useful sensor is the real-time demodulation of the signal waveform. As the signal produced by the sensor is amplitude-modulated, it is not possible to obtain a voltage time-series of a disturbance in the flow directly. It is first necessary to demodulate the signal; a step which can be done in post-processing. While it is feasible to first acquire the sensor signal and then post-process as a second step, it would be more practical if a real-time output could be obtained of the signal in a demodulated state. This is made possible by the implementation of a specialized acquisition system which is designed to demodulated data in real time. This acquisition hardware is produced by the "Gnuradio"[10] organization and is called the "USRP" or Universal Software Radio Peripheral. This devices is developed as an open-source community-

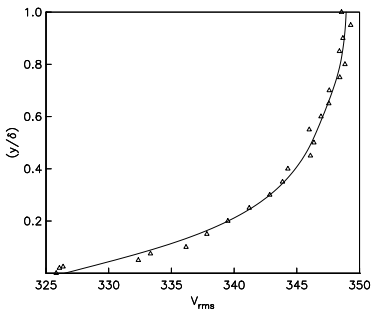

Figure 9. Mean velocity profile in a Mach 1.4 turbulent boundary layer measured with plasma sensor.

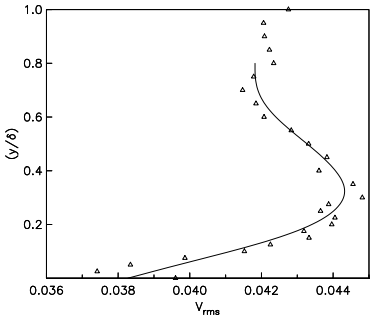

Figure 10. Velocity fluctuation profile in a Mach 1.4 turbulent boundary layer measured with plasma sensor.

driven effort which also develops the optimized software routines necessary to do waveform demodulation in real-time using a host-pc. The hardware consists of a 64 MHz 12-bit digitizer and an Altera Cyclone FPGA and communicates with the pc via USB. The FPGA performs the digital down-conversion of the signal; the rest of the processing is done in software. A screen-capture of the software running in real-time is seen in Figure 11.

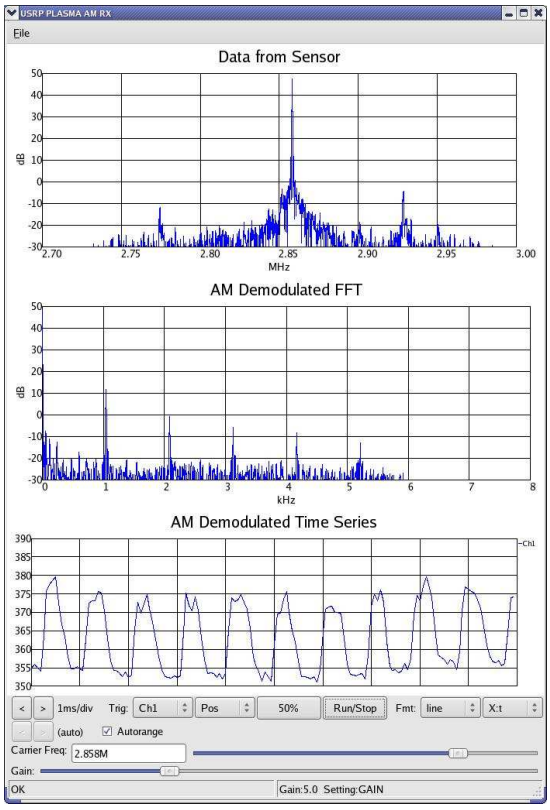

Figure 11. Real-time acquisition and demodulation of plasma anemometer voltage.

The waveform acquired in this case was modulated by a 1 kHz disturbance. The graphical display has three plots. The top plot shows the raw voltage fft in its modulated state; the carrier is clearly seen at 2.858 MHz; it may be just possible to see the sidebands at a distance of 1 kHz from the carrier. The middle plot shows the result of real-time demodulation; the signal is shifted to base-band, the carrier is removed and a low-pass filter applied to remove mirror images. The sideband is now clearly displayed at 1 kHz. The bottom

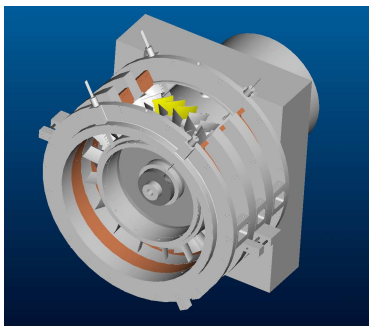

Figure 12. Notre Dame 400 HP Transonic Compressor Facility.

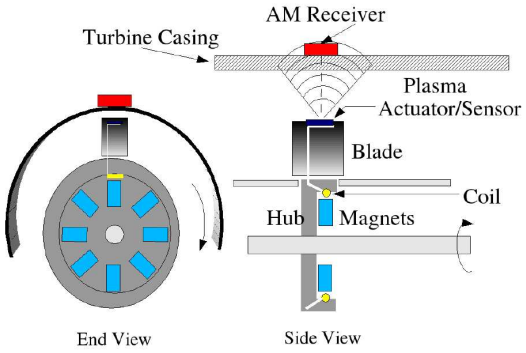

Figure 13. Wireless transmission through turbofan casing.

plot shows the time-series of this demodulated waveform, again in real time. With this real-time acquisition system it is possible to operate the sensor as a device which produces a voltage-times series correlated to the flow dynamics with the details of the amplitude-modulation dynamics hidden from the operator.

VIII. Wireless Transmission

The plasma sensor is driven by a 350 Vrms, 5 Watt signal which produces electro-magnetic energy. This energy, which is broadcast to the surroundings, can be captured wirelessly with a suitable antenna. In the case of the plasma sensor, the transmitting antenna is actually the high-voltage cable that carries the signal to the electrode just beyond the step-up transformer. The receiving antenna can be a simple wire 2 meters in length. This novel feature was demonstrated using the USRP Gnuradio board; the image shown in Figure 11 was actually captured wirelessly at distances greater than 3 meters. Almost no difference was seen in the signal characteristics between the conventional wired-connection mode and the wireless connection mode. This wireless capability opens up interesting applications where it may be difficult to bring out signal wires, such as turbo-machinery. This application is shown in Figures 12 and 13 and is to be tested shortly at Notre Dames Transonic Compressor Facility.

IX. MEMS Scale Design

The plasma anemometer is an ideal candidate for mems-scale fabrication techniques. There are numerous advantages to be had by miniaturizing the probe design. A reduced gap should reduce the voltage required to initiate the plasma. This in turn would decrease the size of the amplifier and transformer required, with the ultimate objective being the use of solid-state devices which could be achievable for run-time voltages of a couple hundred volts. In addition, smaller sensors would provide better spatial resolution, and could be combined in arrays of multiple units for distributed measurements.

An example of the work being done to miniaturize the sensor can be seen in Figure 14. The gap is precisely formed at the tip, and can be made any dimension specified by the designer. An example of this sensor in operation can be seen in Figure 15.

This devices features a 25 μm^2 silicon wafer with a layer of platinum deposited on the surface to form of a pair of electrodes. The gap is designed to be 5μm across. The voltages required to obtain a glow discharge across a gap of this size are on the order of 1/3 of the voltage required by the standard size probes, and it is hoped this can be reduced further as the design is optimized with smaller gaps.

X. Summary and Conclusion

The development of a plasma velocity sensor was successful and has shown significant promise as a robust velocity sensor for high Mach number, high enthalpy tunnel experiments. The plasma probe is sensitive to both the mean and fluctuating components of mass-flux, where the mean state of the sensor is shown by

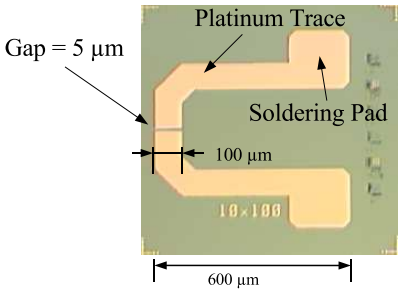

Figure 14. Silicon-based mems surface mount plasma sensor.

Figure 15. Mems scale plasma sensor, 5μm gap, plasma on.

the amplitude of the carrier, and the response to fluctuations is shown in the sidebands at each side of the carrier. Measurements have been made at speeds up to Mach 5. These measurements were conducted at voltages up to 350 V r.m.s..

Analysis of the probe's theory of operation indicate that it should be insensitive to temperature, which makes calibration considerably easier in compressible flows compared to heat transfer based sensors, such as hot-wires.

The sensor offers extremely high frequency response without compensation. Using controlled and documented disturbances, frequencies of up to 200 kHz were directly measured. In principle, an uncompensated frequency response up to the carrier frequency is possible, which for this experiment was as much as 2 MHz. The amplitude modulated a.c. carrier output of the sensor has a signal to noise ratio that is higher than typical hot-wires, and it's high frequency of operations makes it insensitive to common mode noise. It is possible to miniaturize the design using MEMS construction techniques which will reduce the voltage requirement and enable distributed versions of the sensor on surfaces and membranes.

Wireless transmission of the sensor was demonstrated, with a real-time demodulation capability that enabled the output of a voltage time-series of the flow dynamics at distances over 10 feet.

Acknowledgments

This work was supported by a STTR Phase I and Phase II contracts with Innovative Scientific Solutions, Inc. under AFOSR Contract Numbers F49620-03-C-0055 and FA9550-05-C-0022 which are monitored by Dr. John Schmisseur. The U.S. Government is authorized to reproduce and distribute reprints for government purposes not withstanding any copyright therein. The help of Professor P. Fay and Xiang Li of Notre Dame in the fabrication of the mems devices is greatly appreciated.

References

[1]Lindvall, F., "A Glow Discharge Anemometer," AIEE Trans., 1934, f53.

[2]Fucks, W., "Untersunchung der Betreibseigenschaften des Vorstromanemometers," NACA TN-1178, 1944, Translated 1947.

[3]Mettler, R., *The Anemometric Application of an Electrical Glow Discharge in Transverse Air Streams*, Ph.D. thesis, California Institute of Technology, 1949.

[4]Werner, F. D., *The Corona Anemometer and its Application to Study of the Effect of Stilling Chamber Turbulence on Test Section Turbulence in a Wind Tunnel at Mach Number Three.*, Ph.D. thesis, University of Minnesota, 1955.

[5]Vrebalovich, T., *The Development of Direct- and Alternating-Current Glow-Discharge Anemometers for the Study of Turbulence Phenomena in Supersonic Flow.*, Ph.D. thesis, California Institute of Technology, 1954, JPL Report 20-81.

[6]Matlis, E. Corke, T. and Gogineni, S., "A.C. Plasma Anemomter for Hypersonic Mach Number Experiments," AIAA Paper 2006-1245, January 2006.

[7]Post, M. and Corke, T., "Separation Control on High Angle of Attack Airfoil using Plasma Actuators," AIAA Paper 2003-1024, 2003, accepted AIAA J.

[8]Enloe, L., McLauglin, T., CanDyken, R., Kachner, K., Jumper, E., and Corke, T., "Mechanisms and Response of a Single Dielectric Barrier Plasma Actuator," AIAA Paper 2003-1021, 2003.

[9]Loeb, L., *Fundamental Processes of Electrical Discharge in Gases*, John Wiley and Sons, 1939.

[10]"http://gnuradio.org/trac/wiki." .